UNIVERSITY POLITEHNICA OF BUCHAREST

ETTI-B DOCTORAL SCHOOL

Decision No. 534 from 28.07.2020

PhD THESIS
-SUMMARY-

Radar Cross Section Measurements in the Real Environment

Măsurarea suprafeței echivalente radar într-un mediu real

PhD Student: **Mihai Ilie-Valentin**

DISSERTATION COMMITTEE

President	**Prof. Gheorghe Brezeanu**	from	**University POLITEHNICA of Bucharest**
Co-advisor	**Prof. Răzvan Tamaș**	from	**University POLITEHNICA of Bucharest**
Co-advisor	**Prof. Ala Sharaiha**	from	**University of Rennes1**
Reviewer	**Prof. Claire Migliaccio**	from	**University of Côte d'Azur**
Reviewer	**Prof. Tudor Palade**	from	**Technical University of Cluj-Napoca**
Reviewer	**Prof. Ioan Nicolaescu**	from	**Military Technical Academy Ferdinand 1**
Reviewer	**Conf. Alina Bădescu**	from	**University POLITEHNICA of Bucharest**

Bucharest 2020

Abstract

English

Radar cross section (RCS) measurements are generally performed in anechoic chambers or in an open area test site, under far-field conditions. Large targets, such as aircrafts, ships, and other large vehicles cannot be placed inside an anechoic chamber, or the cost of such a measuring site would be prohibitive. Moreover, classical near-field to far-field transformations are complex, time-consuming and expensive to be implemented at a large scale, and therefore not suitable for processing data in a real-time scenario. To overcome these drawbacks, we propose a technique to evaluate the RCS in the Fresnel region in a multipath environment.

An analytical field-zone extrapolation factor is derived; a computing time saving technique with Fresnel integrals is then developed and experimental results are provided by using three different antenna systems: vivaldi, log-periodic and horn antennas. The RCS measurements are performed over simple and complex targets placed in real environment. The distance averaging technique, coupling subtraction and time gating are proposed in order to reduce the effects of the environment. The RCS is evaluated also at high incidence agles by taking into account the effects of the diffraction.

Română

Măsurătorile suprafeței echivalente radar (SER) sunt, în general, efectuate în camere anecoide sau într-o zonă deschisă, în condiții de câmp îndepărtat. Țintele mari, precum avioanele, navele maritime și alte vehicule nu pot fi plasate în interiorul unei camere anecoide sau costurile configurației de măsură devin prohibitive. Mai mult decât atât, transformările clasice din câmp apropiat în câmp îndepărtat sunt complexe, consumatoare de timp și costisitoare pentru a fi implementate la scară largă și, prin urmare, nu sunt adecvate într-un scenariu în timp real. Pentru a depăși aceste dezavantaje, în această teză propunem o nouă tehnică de evaluare a suprafeței echivalente radar în regiunea Fresnel și într-un mediu real.

Un factor analitic de extrapolare a zonei de câmp este derivat; apoi este dezvoltată o tehnică de calcul rapid cu integrale Fresnel, iar rezultatele experimentale sunt obținute folosind trei sisteme de antene diferite: Vivaldi, log-periodice și horn. Măsurătorile SER-ului sunt efectuate pe ținte simple și complexe plasate într-un mediu real. Pentru a reduce efectele mediului real, sunt propuse tehnica medierii în distanță, reducerea cuplajului mutual și ferestruirea în domeniul timp. SER-ul este evaluat și la unghiuri de incidență ridicate, luând în considerare efectele difracției.

Contents

1. Introduction

1.1 Presentation of the PhD domain

Radar cross section (RCS) evaluation is made in anechoic chambers or in an open area test site (OATS), under far-field conditions. Large targets, such as aircrafts, frigates and other large vehicles cannot be placed inside an anechoic chamber, or the cost of such a measuring site would be prohibitive. Conversely, RCS measurements at far-field ranges in an OATS are faced to ground reflections and a low signal-to-noise ratio (SNR). Moreover, classical near-field to far-field transformations are complex, time-consuming and expensive to be implemented at a large scale, and therefore not suitable for processing data in a real-time scenario. In that case, techniques for RCS evaluation from measurements at Fresnel region radar-to-target distances in a perturbed, multipath environment might be needed. The radar cross section of large, complex targets can also be evaluated on small scale models.The far-field, radar cross section of a simplified model consisting of rectangular patches and slots can be computed analytically; it may therefore serve as a reference for comparison purposes when extracting the RCS by processing Fresnel-zone data.

1.2 The purpose of the thesis

RCS measurements are generally performed in anechoic chambers, but the sizes of the chambers must exceed the far-field zone limit and the absorbers must become effective to the lower end of the frequency range of interest. These constraints are difficult to respect for a large target and/or when the RCS must be evaluated at low frequencies. Current researches of the RCS evaluation of large targets in the real environment take into account the reduction of the effects of multipath propagation; a typical case of interest consists in measuring the RCS of a ship in a multipath environment, such as the sea surface. In order to calibrate the measurements, reflectors with known electromagnetic signature are attached to the ship. However, such a method is quite expensive because the measurements are performed with a helicopter. Obtaining encouraging results for the gain of the antennas and the parameters of the materials, a potentially applicable technique would be the distance averaging approach.

1.3 Thesis content

The Ph.D. dissertation is organized in 6 chapters:

Chapter 1 presents the general introduction of the thesis, the PhD domain and the purpose of the thesis.

Chapter 2 presents an overview on the principles of the radar cross section, in addition to a state of the art for the theory. The chapter starts with the basic equations that govern the radar equation. The radar cross section phenomenology is

explained and the RCS prediction methods are presented together with a literature review.

In chapter 3, we present a theoretical approach to evaluate the RCS of a rectangular target in the Fresnel and far-field zones and an analytical field-zone extrapolation factor is derived; a computing time saving technique with Fresnel integrals is then developed and experimental results are provided by using three different antenna systems: vivaldi, log-periodic and horn antennas. The RCS measurements are performed in real environment and the distance averaging technique and coupling subtraction are proposed in order to reduce the effects of the environment and of the multipath propagation.

An Ultra-Wide Band (UWB) physical optics approach for Fresnel region RCS of several complex targets at non-normal incidence angles is proposed in chapter 4. Firstly, a mathematical model is developed to evaluate the RCS of both a rectangular and circular target. Further, the mathematical model for simple targets is improved for the evaluation of the RCS of a simplified, scale model of a camping car side, a simplified model of a frigate side and a scale model of a container house. Moreover, the time-gating technique is proposed also to reduce the reflexions and the effects of the real environment. The measurement protocol and experimental results with horn antennas are provided.

A further improvement of the method is presented in chapter 5 by taking into account the effects of the diffraction at the edges of targets. The mathematical model presented in chapter 3 and 4 is extended to high oblique incidence angles by using the uniform theory of the diffraction. Experimental results are provided for a rectangular target and for a complex target.

Finally, in the chapter 6 the work is concluded, the results and the original contributions are highlighted and perspectives are drawn towards the future progress that could be done.

2. Radar cross section principles

2.1 Introduction

In this chapter we present a brief review on the theory of the radar cross section and its corresponding methods. The basic formulation of these methods is given. Moreover, we present a literature review on the different applications of the RCS in the far-field and Fresnel region.

2.2 The radar range equation

The radar range equation (RRE) is the most used mathematical relationship in the analysis of the radar cross section of various targets.

In the simple case of detection of a target, a required minimum signal-to-noise ratio can be defined, based on the required detection probability, target statistics, and radar characteristics. Because receiver noise can be considered to have a constant average power, the minimum signal-to-noise ratio defines the minimum level of received signal, P_{rmin}, that can be tolerated. Therefore, the maximum detection range is given by

$$R_{max} = \sqrt[4]{\frac{P_t G^2 \lambda^2 \sigma}{(4\pi)^3 P_{rmin}}} \qquad [m], \tag{2.1}$$

where P_t is the transmitted power, λ is the wavelength, G is the gain of the radar antennas, R_{max} is the distance between radar and target and σ is the radar cross section of the target.

2.3 Radar cross section phenomenology

The IEEE defines RCS as a measure of reflective strength of a target defined as the ratio of the power scattered in a specific direction to the power per unit area in a plane wave incident on the scatterer from a specific direction. More precisely, it is the limit of that ratio as the distance from the scatterer to the point where the scattered power is measured approaches infinity,

$$\sigma = \lim_{r\to\infty} 4\pi r^2 \frac{|\mathbf{E}_r|^2}{|\mathbf{E}_i|^2} = \lim_{r\to\infty} 4\pi r^2 \frac{|\mathbf{H}_r|^2}{|\mathbf{H}_i|^2}, \tag{2.2}$$

where $\mathbf{E}_r$ and $\mathbf{H}_r$ is the electric and magnetic scattered field and $\mathbf{E}_i$ and $\mathbf{H}_i$ is the electric and magnetic field incident at the target.

2.4 RCS prediction techniques

Perhaps the oldest and easiest technique to estimate the RCS is the geometric optics method originally applied to light. Even in bistatic configurations the radar cross

section is given by a simple formula that only includes the local curvature radius at the specular level. However, this basic procedure fails when one or both curvature radii are infinite, as in the case of a cylindrical or a flat surface, and then one might have to switch to the physical optics approach. The surface curvature radius may be infinite, but physical optics give the correct result if the target is not too small and the direction of scattering is not too far from the specular direction. Physical optics can, however, fail at wide angles from the normal direction.

Physical optics actually fails if edge contributions are neglected, and at this stage one should invoke Keller's geometrical theory of edge diffraction [1] (GTD). GTD is based on the standard wedge diffraction approach which offers remarkably good results for a wide range of scattering issues. It is, though, a wide-angle method, but it works within the limits of the shadow and reflection boundaries. Uniform asymptotic approaches have been developed [2] to solve these limitations, but GTD suffers yet another shortcoming, yielding infinite results at caustics.

The Method of Equivalent Currents (MEC) was introduced to solve the caustic problems of GTD [3], but the technique does not solve the singularities of the diffraction coefficients. Ufimtsev formulated the physical theory of diffraction (PTD) for analyzing the edges [4].

Some of the earliest studies on RCS estimation for simple shapes were published since 1965 [5, 6, 7, 8, 9, 10, 11]. The RCS evaluation of military targets, airplanes an missiles has been studied since the beginning up to now [12, 13, 14, 15, 16].

2.5 RCS analysis in the Fresnel region

Measurement of the far-field RCS is possible by means of a far-field test range, where the distance radar-target is such, that the far-field condition is satisfied, or by means of a compact test range, where a quasi-plane wave is synthesized and illuminated upon a target. A disadvantage of the far-field ranges is their length, which becomes long as the radar's antenna aperture grows. The compact test range size is also big, provided its quiet zone is big in order to accommodate the target. All of the mentioned measurement options require quite an expensive infrastructure, which is not always available especially for start-up companies. A solution is the measurement of the Fresnel region RCS in a planar Fresnel region scanning system, a few wavelengths away from the antenna aperture and a subsequent forward propagation of the measured Fresnel region to far-fields. In the literature, there are plenty methods to analyze the Fresnel region RCS.

In this chapter the theory of the radar cross section and some methods of analysis were presented. A literature review on the application of RCS in the military and civilian fields of interest was also presented, showing that Fresnel region RCS has become a very useful approach in many actual scenarios. However, all the methods presented above were tested in anechoic chambers or in open area test sites and therefore a real environment validation is required.

3. A new technique to measure the RCS in the Fresnel region and real environment using Vivaldi, log-periodic and horn antennas

3.1 Overview

Far-field RCS measurements face several challenges: ground reflections, a low signal-to-noise ratio (SNR) for the reflected wave [17], a complex radar system [18] and near-field to far-field transformations that might be complex, time-consuming and expensive to be implemented at a large scale, and therefore not suitable for a real-time scenario [19].

In order to overcome these shortcomings, methods for determining the far-field RCS at Fresnel region distances have been developed recently and presented in the last chapter [20].

3.2 Analytical evaluation of the RCS in the Fresnel region

The RCS is defined as

$$\sigma = 4\pi r^2 \frac{|\mathbf{H}_r|^2}{|\mathbf{H}_i|^2}, \tag{3.1}$$

where r is the range or radar-to-target distance, $\mathbf{H}_i$ and $\mathbf{H}_r$ are the incident and the reflected magnetic field strength at the radar.

The magnetic field reflected by a rectangular plate of a size a by b can be expressed as follows:

$$H_r = \int_{-\frac{b}{2}}^{\frac{b}{2}} \int_{-\frac{a}{2}}^{\frac{a}{2}} j\frac{kJ_S}{4\pi r}\exp[-jk(r+\Delta r)]\mathrm{d}x\prime\mathrm{d}z\prime, \tag{3.2}$$

where Δr is the path length difference in the phase term.

The current density J_S on the surface of a rectangular, metallic plate in a radar-type setup such as in fig. 3.1 could be approximated using the physical optics (PO) approach:

$$\mathbf{J}_S = \begin{cases} 2\mathbf{n} \times \mathbf{H}_i, & \text{in the specular region} \\ 0, & \text{in the shadowed region.} \end{cases} \tag{3.3}$$

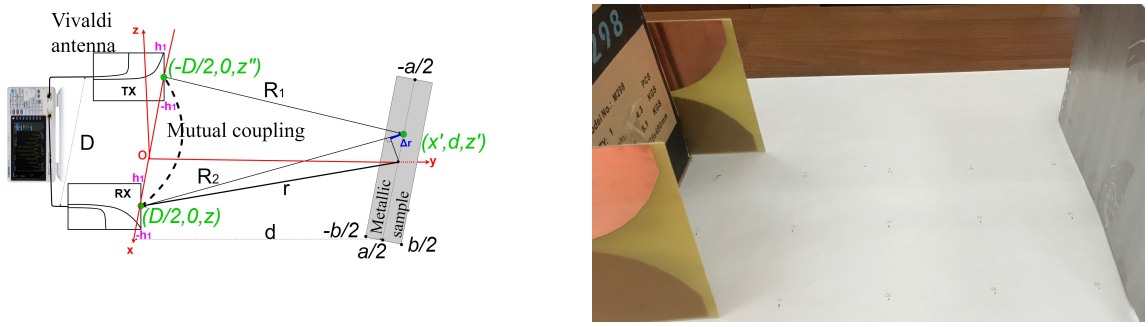

(a) (b)

Figure 3.1: Radar-type setup with Vivaldi antennas (a) schematic representation (b) real measurement configuration.

In order to take into account all the contributions of the source points on the transmitting antenna aperture, and of the field points on the receiving antenna aperture, an average over both apertures can be computed:

$$\sigma = \frac{4\pi}{\lambda^2}\left|\frac{1}{(2h_1)^2}\int_{-h_1}^{h_1}\int_{-h_1}^{h_1}\int_{-\frac{b}{2}}^{\frac{b}{2}}\int_{-\frac{a}{2}}^{\frac{a}{2}}\exp(-jk\Delta r)\mathrm{d}x\prime\mathrm{d}z\prime\mathrm{d}z\mathrm{d}z\prime\prime\right|^2. \tag{3.4}$$

The resulting integrals of type

$$\int \exp\left(-jk_0\frac{x\prime^2}{d}\right)\mathrm{d}x\prime = \int \exp\left[-j\left(\sqrt{\frac{k_0}{d}}x\prime\right)^2\right]\mathrm{d}x\prime \tag{3.5}$$

are actually Fresnel integral i.e., $f(w) = \int_w^\infty \exp(-ju^2)\mathrm{d}u$. The expression of the RCS is eventually found as

$$\begin{aligned}\sigma_{Fr} = \frac{4\pi}{\lambda^2}\Bigg\{\sqrt{\frac{d}{k_0}}\Bigg|f\left(-\frac{a}{2}\sqrt{\frac{k_0}{d}}\right) - f\left(\frac{a}{2}\sqrt{\frac{k_0}{d}}\right)\Bigg|\frac{1}{(2h_1)^2}\frac{2d}{k_0}\Bigg|\int_{-\frac{b}{2}}^{\frac{b}{2}}\Bigg[f\left(-h_1\sqrt{\frac{k_0}{d}} - \\ - z\prime\sqrt{\frac{k_0}{d}}\right) - f\left(h_1\sqrt{\frac{k_0}{d}} - z\prime\sqrt{\frac{k_0}{d}}\right)\Bigg]^2\mathrm{d}z\prime\Bigg|\Bigg\}^2 = \frac{4\pi Q^2}{\lambda^2}.\end{aligned} \tag{3.6}$$

By using our RCS form as in (3.6) instead of the four-integral form (3.4) the computing time effort can be reduced from a couple of hours to a few seconds. The reduction in computing time comes both from the reduction of the integration order, and from utilizing an asymptotic form for computing the Fresnel integrals.

3.3 Analytical evaluation of the RCS in the far-field zone

At far-field distances, when $d \to \infty$, the RCS expressed with (3.6) for the case of linear aperture antennas (Vivaldi antennas) becomes

$$\sigma_{ff} = \frac{4\pi a^2 b^2}{\lambda^2}. \tag{3.7}$$

3.4 Field-zone extrapolation factor between Fresnel and far-field region

A field-zone extrapolation factor F from Fresnel region to far-field can be defined as the ratio between Fresnel region RCS (3.6) and far-field RCS (3.7):

$$F = \frac{\sigma_{Fr}}{\sigma_{ff}} = \frac{Q^2}{a^2 b^2}. \tag{3.8}$$

3.5 Calibration

In this section there are proposed 3 calibration techniques for radar-type configurations: a radar antennas group-delay, gain and mutual coupling.

In a practical RCS measurement setup, the group delay introduced by the two antennas should be found, in order to accurately assess the range when modeling the real setup by an equivalent setup with point-like antennas placed in the group delay origin of the actual antennas.

A gain calibration should also be performed prior to RCS measurements, provided that low directivity antennas are generally used at low frequencies e.g., in the L-band. In that case, the presence of one antenna close to the other not only results in a mutual coupling, but it also impacts on the radiation pattern and gain figure.

In the case of low-directivity antennas, such as Vivaldi, in a quasi-monostatic configuration as in fig. 3.1 there is a strong mutual coupling between antennas. Subtracting the mutual coupling, one can reduce also the effects of the real environment.

3.6 Measurement protocol

The ratio $\frac{P_r}{P_t}$ from the radar equation can be extracted from the S_{21} parameter. Additionally, impedance mismatches corrections can be included in the expression of the power link budget. The mutual coupling between antennas can be reduced by subtracting the magnitudes of S_{21} measured with and without the target. Therefore,

$$\sigma_{far-field} = \frac{(4\pi)^3}{FG^2\lambda^2} \frac{|S_{21_{Fr}}^{total} - S_{21}^{coupling}|^2}{|1 - S_{22}|^2} \frac{R_0}{R_a(1 - |S_{11}|^2)}, \tag{3.9}$$

where, F is the field-zone extrapolation factor, R_0 is the normalizing impedance (50 ohm), R_a is the radiation resistance of the receiving antenna, G is the gain of each

antenna, $S_{21}^{coupling}$ is the S_{21} parameter measured without the target and $S_{21_{Fr}}^{total}$ is a normalized transfer function computed as an average figure over the set of distances d_n in the Fresnel region.

A normalized, distance averaged transfer function $S_{21_{Fr}}^{total}$ can be used in order to compensate the effects of the multipath propagation for measurements in a real environment [21]:

$$S_{21_{Fr}}^{total} = \frac{1}{N}\sum_{n=1}^{N}\left(\frac{d_n}{d_0}\right)^2 \left| S_{21,n}\exp(2jkd_n)\right|, \tag{3.10}$$

where d_0 is a reference distance usually set at 1 m.

3.7 Antennas parameters

In this section are presented and measured the parameters of the antennas, such as the impedance matching and the gain of the antennas.

3.8 Experimental results

In order to validate the method, simulations and measurements were performed at frequencies between 1 and 3 GHz. We took as a target a rectangular, metallic plate of 22 cm by 36 cm. We tested a pair of two identical Vivaldi dipoles of 17.8 cm by 21.04 cm in size.

A vector network analyzer (VNA) was used for measuring the scattering parameters of the system in a real, multipath environment. As a multipath environment we employed an ordinary office room inside a building. In order to find the RCS with (3.9), S_{21}, S_{11}, S_{22} should be measured. The S_{21} parameter was measured for seven ranges, i.e. 40 cm, 50 cm, 60 cm, 70 cm, 80 cm, 90 cm and 100 cm all at the upper limit of the Fresnel region at frequencies between 1 and 3 GHz. A normalized average over the set of S_{21} parameters was computed as in (3.10), in order to reduce the effects of the multipath propagation.

Fig. 3.2a, display the RCS results and fig. 3.2b show the error vector (the Fresnel region RCS corrected with the field-zone extrapolation factor F to far-field RCS ratio).

In this chapter, a novel method to estimate the Fresnel region RCS for the particular case where antenna and target sizes are in the same order as the radar-target distances was proposed. Field averaging over the antenna apertures results in accurate RCS values as long as the receiving antenna is quasi-uniformly illuminated by the target and the current distribution over the transmitting antenna can be assumed as constant. The error figure with respect to the theoretical, far-field RCS rarely exceeds 2 dB both for measurements with Vivaldi and log-periodic antennas in an anechoic chamber, in real environment and for simulations. Other RCS validations with log-periodic and horn antennas are presented in the full thesis manuscript.

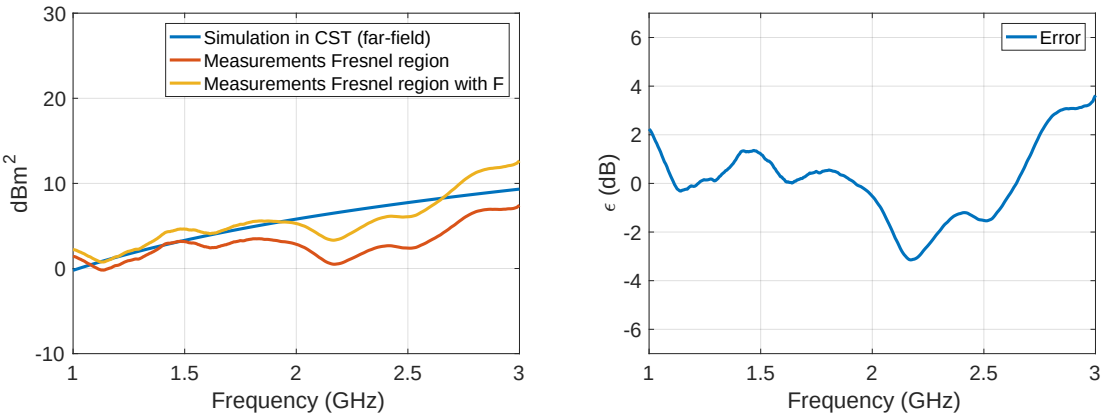

(a) (b)

Figure 3.2: RCS results obtained with Vivaldi antennas in a multipath, real-environment (a) and Fresnel region RCS (3.9) to theoretical far-field RCS (3.7) ratio (error vector) (b)

4. Radar cross section measurements on complex targets at non-normal incidence angles

4.1 Overview

The phase deviation between the contributions of different source points to the scattered field should be calculated, in order to find the RCS of a target using PO. Such an evaluation is more difficult in the Fresnel region due to the reactive components of the field and the complexity of the surface integrals to be computed. Several approaches have been proposed, in order to overcome these shortcomings when computing the phase deviation at short distances through modified Green functions [22] or approximations in the phase term [23].

4.2 Analytical evaluation of the RCS at oblique incidence

4.2.1 Case of a rectangular plate

Fresnel region

By averaging the field distribution over the apertures of both antennas, the RCS at ranges in the Fresnel region is found as:

$$\sigma_{Fr} = \frac{4\pi\cos^2\theta}{\lambda^2}\left|\frac{1}{(2h_1)^4}\int_{-h_1}^{h_1}\int_{-h_1}^{h_1}\int_{-h_1}^{h_1}\int_{-h_1}^{h_1}\int_{-\frac{b}{2}}^{\frac{b}{2}}\int_{-\frac{a}{2}}^{\frac{a}{2}}\exp\left[-jk\left(\frac{(z-z')^2}{2d}+\frac{(z''-z')^2}{2d}+\frac{(z')^2}{2d}\right.\right.\right.$$
$$\left.\left.\left.+\frac{\Big(x'-(x''-h_1)\Big)^2}{2d}+\frac{\Big(x'-(x+h_1)\Big)^2}{2d}+2z'\sin\theta\right)\right]\mathrm{d}x'\mathrm{d}z'\mathrm{d}z\mathrm{d}z''\mathrm{d}x\mathrm{d}x''\right|^2 = \frac{4\pi\cos^2\theta}{\lambda^2}Q_{Fr}^2. \tag{4.1}$$

Far-field

The PO, far-field expression of the RCS of a plate, σ_{ff} can be found from (4.1) when $d \to \infty$:

$$\sigma_{ff} = \frac{4\pi\cos^2\theta}{\lambda^2}\left|\int_{-\frac{b}{2}}^{\frac{b}{2}}\int_{-\frac{a}{2}}^{\frac{a}{2}}\exp(-2jkz'\sin\theta)\mathrm{d}x'\mathrm{d}z'\right|^2 = \frac{4\pi a^2b^2\cos^2\theta}{\lambda^2}\left[\frac{\sin(kb\sin\theta)}{kb\sin\theta}\right]^2. \tag{4.2}$$

Field-zone extrapolation factor

An analytical field-zone extrapolation factor F from Fresnel to far-field region can be defined:

$$F = \frac{\sigma_{Fr}}{\sigma_{ff}} = \frac{Q^2_{Fr_{plate}}}{a^2 b^2 \left[\frac{\sin(kb\sin\theta)}{kb\sin\theta}\right]^2}. \tag{4.3}$$

4.2.2 Case of a circular target

Fresnel region

By expressing Δr and averaging the field distribution over the apertures of the transmitting and receiving antenna, an average over both apertures can be computed and the analytical RCS at Fresnel region is finally found as:

$$\sigma_{Fr} = \frac{4\pi\cos^2\theta}{\lambda^2}\left|\frac{1}{(2h_1)^4}\int_{-h_1}^{h_1}\int_{-h_1}^{h_1}\int_{-h_1}^{h_1}\int_{-h_1}^{h_1}\int_0^a\int_0^{2\pi} a_r \exp\left[-jk\left(\frac{(z-a_r\sin\alpha)^2}{2d}+\right.\right.\right.$$
$$\frac{(z''-a_r\sin\alpha)^2}{2d}+\frac{(a_r\sin\theta)^2}{2d}+\frac{\left(a_r\cos\alpha-(x''+h_1)\right)^2}{2d}+\frac{\left(a_r\cos\alpha-(x-h_1)\right)^2}{2d}+$$
$$\left.\left.\left.2a_r\sin\alpha\sin\theta\right)\right]\mathrm{d}\alpha\mathrm{d}a_r\mathrm{d}z\mathrm{d}z''\mathrm{d}x\mathrm{d}x''\right|^2 = \frac{4\pi\cos^2\theta Q^2_{Fr}}{\lambda^2}. \tag{4.4}$$

Far-field

The far-field PO expression of the RCS of a circular target is found when $d \to \infty$:

$$\sigma_{ff} = \frac{4\pi\cos^2\theta}{\lambda^2}\left|\int_0^a\int_0^{2\pi} a_r \exp(-2jka_r\sin\alpha\sin\theta)\mathrm{d}\alpha\mathrm{d}a_r\right|^2. \tag{4.5}$$

Field-zone extrapolation factor

An analytical field-zone extrapolation factor F between Fresnel region and far-field can be defined,

$$F = \frac{\sigma_{Fr}}{\sigma_{ff}} = \frac{Q^2_{Fr}}{\left|\int_0^a\int_0^{2\pi} a_r \exp(-2jka_r\sin\alpha\sin\theta)\mathrm{d}\alpha\mathrm{d}a_r\right|^2}, \tag{4.6}$$

as a ratio between analytical Fresnel region RCS (4.4) and far-field PO RCS (4.5).

4.2.3 Case of a simplified, small scale model of a camping car side

Fresnel region

The magnetic field $H_{r_{c-c}}$ reflected by a small scale model of a camping car side (fig. 4.1) at a distance d can be expressed as follows:

$$H_{r_{c-c}} = H_r - H_{r_1} - H_{r_2} - H_{r_3} - H_{r_4} - H_{r_5} = j\frac{k\exp(-jkd)}{4\pi d} J_S \cos\theta Q_{FR_{c-c}}. \quad (4.7)$$

(a) (b)

Figure 4.1: Camping car side as a complex target (a) real target and (b) small scale model

Therefore, the RCS of the simplified, small scale model of a camping car side at ranges in the Fresnel region is found as

$$\sigma_{Fr} = 4\pi d^2 \left| \frac{H_{r_{c-c}}}{H_i} \right|^2 = \frac{4\pi\cos^2\theta}{\lambda^2} \left| \frac{1}{(2h_1)^4} \int_{-h_1}^{h_1}\int_{-h_1}^{h_1}\int_{-h_1}^{h_1}\int_{-h_1}^{h_1} Q_{FR_{c-c}} \mathrm{d}x\mathrm{d}z\mathrm{d}x''\mathrm{d}z'' \right|^2. \quad (4.8)$$

When $d \to \infty$, the PO, far-field RCS of the simplified, small scale model of a camping car side σ_{ff} is found:

$$\sigma_{ff} = \frac{4\pi\cos^2\theta(a^2b^2 - S_1)}{\lambda^2}, \quad (4.9)$$

where

$$\begin{aligned} S_1 =& (b/2 - b_{11})^2(a_1 - a_{11})^2 + (b_2 - b_{22})^2(a_2 - a_{22})^2 + (b_3 - b_{33})^2(a_3 - a/2)^2 + \\ & (b_4 - b_{44})^2(a_4 - a/2)^2 + (b_5 - b_{55})^2(a_5 - a_{55})^2 \end{aligned} \quad (4.10)$$

and a_i, a_{ii} and b_i, b_{ii} with $i \leq 5$ are the sizes of the windows and of the wheels.

Field-zone extrapolation factor

The field-zone extrapolation factor F from Fresnel to far-field zone is eventually found as

$$F = \frac{\sigma_{Fr}}{\sigma_{ff}}. \tag{4.11}$$

4.2.4 Case of a simplified, small scale model of a frigate side

In order to analyze the RCS of a frigate (fig. **??**), a simplified, small scale model consisting of 17 rectangular patches was entered in CST. The total magnetic field reflected by the model of the frigate is obtained by adding the magnetic field reflected by each rectangular patch.

When $d \to \infty$, the PO, far-field RCS of the simplified, small scale model of a frigate side σ_{ff} is determined and then the field-zone extrapolation factor F from Fresnel to far-field zone is found as

$$F = \frac{\sigma_{Fr}}{\sigma_{ff}}. \tag{4.12}$$

4.2.5 Case of a scale model of a container house

In order to analyze the RCS of a container house (fig. 4.2b), a small scale model was entered in CST. The total magnetic field reflected by the model of the container house is obtained by subtracting the magnetic field that would be reflected by five rectangular patches corresponding to the non-reflective surface of the windows and door from the field scattered by the two large rectangular patches corresponding to the front wall and the roof.

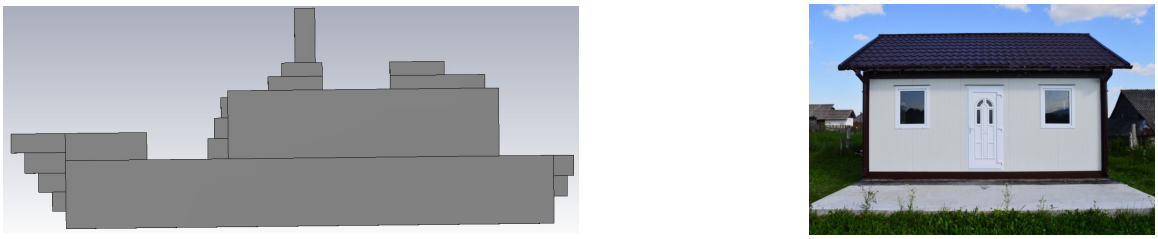

(a) (b)

Figure 4.2: A simplified, small scale model of the frigate constructed by rectangular patches (a) and a container house (b).

Far-field

When $d \to \infty$, the PO, far-field RCS of the complex target σ_{ff} is found and the field-zone extrapolation factor F from Fresnel to far-field zone is eventually written as follows

$$F = \frac{\sigma_{Fr}}{\sigma_{ff}}. \tag{4.13}$$

4.3 Measuring protocol

The method was validated by measurements at normal incidence ($\theta = 0°$) and at incidence angles within the limits of the PO approximation ($\theta \leq 20°$).

We choose as a target a rectangular plate of a size $a = 36$ cm by $b = 22$ cm, a disk with radius 15 cm, a simplified, small scale model of a camping car side, a simplified, small scale model of a frigate side and a small scale model of a container house side.

The targets were placed in a real multipath environment and the measurements were performed at frequencies between 2 and 10 GHz. A set of identical horn antennas of 15 cm by 15 cm in aperture size was used to measure the S_{21} parameter at a set of Fresnel region antenna-to-target distances, i.e. $d = 40$ cm, 50 cm, 60 cm, 70 cm, 80 cm, 90 cm and 100 cm.

4.4 Time gating

Some studies introduced time gating as an alternative technique to reduce the influence of the real environment and mutual coupling between Tx and Rx antennas on a quasi monostatic radar link.

Time gating is considered in this section, as a method to reduce the effect of late reflections in the real environment where measurements are carried out.

The measured S_{21} parameters were transformed into time domain by performing an Inverse Fourier transformation,

$$s_{21}(t) = \mathcal{F}\left\{S_{21}(\omega))\right\}. \tag{4.14}$$

In the time domain, one can discriminate the reflection from the target and the late reflections from other objects in the area. In this case, one can gate out the target reflection and return back to the frequency domain:

$$\{S_{21}(\omega))\} = \mathcal{F}(s_{21}(t)). \tag{4.15}$$

4.5 Experimental results

Figure 4.3 displays a comparison between RCS figures simulated in CST and measured at Fresnel region distances with and without correcting for the field zone with the extrapolation factor F (after coupling subtraction or time gating).

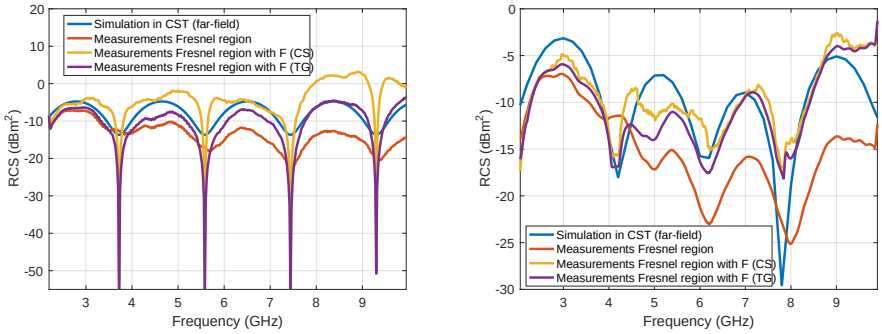

Figure 4.3: A comparison between the RCS results for a rectangular plate at $\theta = 20°$ (a) and for a small scale model of a camping car side at $\theta = 20°$ (b)

We proposed a PO technique for RCS evaluation on simple and several complex targets in the Fresnel zone, suitable both for normal and non-normal incidence.

The field-zone issue was addressed by defining a field-zone extrapolation factor. Complex targets can be approximated by a mesh of rectangular patches and slots; we therefore proposed a method for RCS evaluation based on summing the contributions of the patches to the total field, and on subtracting the contributions of the slots, respectively.

5. Radar cross section evaluation at high incidence angles

5.1 Overview

To overcome the limitation of PO, the effects of the diffraction at the edges of the target should be taken into account. Under the assumptions in the geometrical theory of diffraction (GTD), Keller [1] calculated two diffraction coefficients for a perfectly conducting wedge illuminated by plane, cylindrical, conical and spherical waves. Later, by applying the uniform theory of diffraction (UTD), Kouyoumjian [2] developed diffraction coefficients which remain valid in the transition regions adjacent to shadow and reflection boundaries, where the diffraction coefficients of Keller's original theory fail. By defining equivalent currents [24], the diffracted field can be computed for scattering directions outside of the Keller cone.

5.2 Methodology

Figure 5.1 displays the current distribution when an incident z-polarized wave illuminates a rectangular plate. With r the radar to target distance and $r \to \infty$, the RCS can be defined as

$$\sigma_{PO} = 4\pi r^2 \left| \frac{H_r}{H_i} \right|^2, \tag{5.1}$$

where H_r is the reflected magnetic field and H_i is the incident magnetic field. By taking into account the contribution of the diffraction at the edges of the plate, the RCS can be expressed as

$$\sigma_{difr} = 4\pi r^2 \left| \frac{H_r + H_d}{H_i} \right|^2. \tag{5.2}$$

In fig.5.1, $\mathbf{S}_i$ and $\mathbf{S}_r$ are the Poynting vectors, $\mathbf{E}_i^z$ is the incident electric field, $\mathbf{E}_r$ is the reflected electric field, $\mathbf{H}_d^x$ is the diffracted magnetic field, $\mathbf{E}_d^z$ is the diffracted electric field, $\mathbf{n}$ is the normal vector to the surface of the target and θ is the incidence angle. The upper indexes x and z refer to field sources i.e., the magnetic and electric current distributions I_z and M_x, respectively.

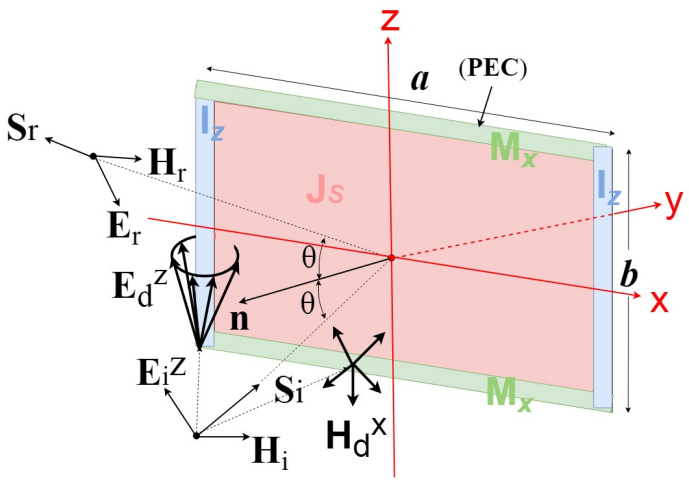

Figure 5.1: Current distribution on a rectangular plate

$$\sigma_{difr} = \left(\sqrt{\sigma_{PO}} + \left| \frac{H_d}{H_i} \right| \sqrt{4\pi r^2} \right)^2, \tag{5.3}$$

where H_d is the diffracted magnetic field.

If the distance r falls within the Fresnel zone, then

$$\sigma_{difr_{Fr}} = \left(\sqrt{\sigma_{PO}}_{Fr} + \left| \frac{H_d}{H_i} \right|_{Fr} \sqrt{4\pi r^2} \right)^2. \tag{5.4}$$

5.3 Case of a rectangular target

5.3.1 Determination of the diffracted-to-incident field ratio

Fresnel region

By using the theory of equivalent currents and the theory of the UTD, the unknown ratio between the diffracted field and the incident field can be expressed as follows:

$$\begin{aligned} \left. \frac{H_d}{H_i} \right|_{Fr} = & -2\sqrt{\frac{k_0}{4\pi}} \frac{\exp\left[-j(k_0 r - \pi/4)\right]}{r} \left\{ \cos\theta D_h \sqrt{\frac{2r}{k_0}} \left[f\left(-\frac{a}{2}\sqrt{\frac{k_0}{2r}} \right) - f\left(\frac{a}{2}\sqrt{\frac{k_0}{2r}} \right) \right] \right. \\ & \left. + D_s \sqrt{\frac{2r}{k_0}} \left[f\left(-\frac{b}{2}\sqrt{\frac{k_0}{2r}} \right) - f\left(\frac{b}{2}\sqrt{\frac{k_0}{2r}} \right) \right] \right\}. \end{aligned} \tag{5.5}$$

Far-field

At far-field distances, the expression of the ratio between the diffracted field and incident field can be written as follows:

$$\left.\frac{H_d}{H_i}\right|_{ff} = \frac{2(H_{dh}|_{ff} + H_{ds}|_{ff})}{H_i}, \tag{5.6}$$

where H_{dh} is the hard diffracted magnetic field and H_{ds} is the soft diffracted magnetic field.

5.3.2 Field-zone extrapolation factor for the diffracted field

The factor for extrapolating the field from Fresnel to far-field zone can be defined as

$$\sqrt{F} = \frac{\sqrt{\sigma_{PO}}_{Fr} + \left|\frac{H_d}{H_i}\right|_{Fr}\sqrt{4\pi r^2}}{\sqrt{\sigma_{PO}}_{ff} + \left|\frac{H_d}{H_i}\right|_{ff}\sqrt{4\pi r^2}}. \tag{5.7}$$

5.4 Case of a complex target

In order to take into account the effects of the diffraction at the edges of the camping car side, the $\frac{H_d}{H_i}$ ratio will be approximated as in the case of a rectangular target.

5.5 Measuring setup

The measurements were performed in the same condition as in the previous chapters. The method was validated by measurements at incidence angles exceeding the 20° limit generally accepted for the PO approximation, i.e. $\theta = 30°$, $\theta = 35°$, 40° and 45°. We choose as a target a rectangular plate of a size $a = 36$ cm by $b = 22$ cm and a simplified small scale model of a camping car side. The target was placed in a real multipath environment and the measurements were performed at frequencies between 2 and 10 GHz.

5.6 Experimental results

Figures 5.2a and 5.3a display the inverse Fourier transform of the S_{21} parameters and 5.2b and 5.3b display a comparison between the RCS resulting from simulations, the RCS measured at Fresnel region distances and the RCS measured at Fresnel region distances corrected with the field-zone extrapolation at $\theta = 45°$ for a rectangular plate and $\theta = 45°$ for a simplified small scale model for a camping car side.

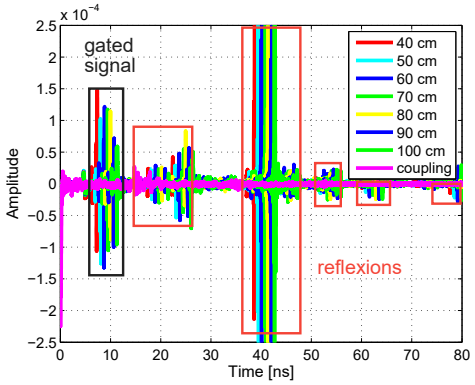

(a) ($\theta = 45°$)

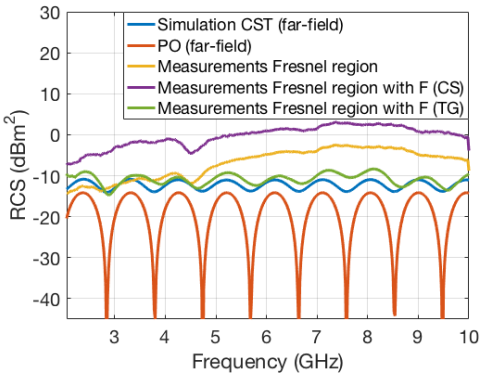

(b) ($\theta = 45°$)

Figure 5.2: Rectangular target - the inverse Fourier transform of the S_{21} parameters at $\theta = 45°$ (a) and a comparison between the RCS results at $\theta = 45°$ (b).

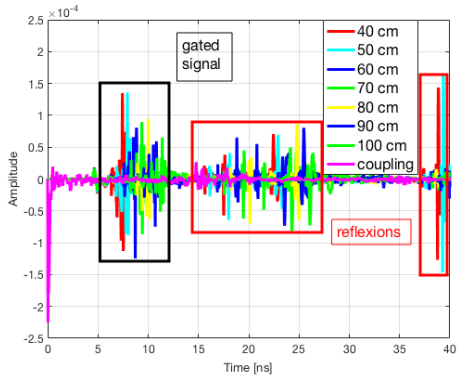

(a) ($\theta = 45°$)

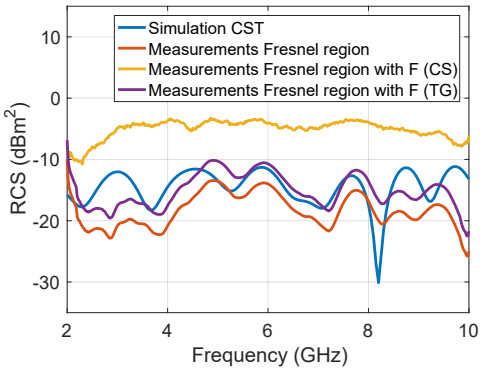

(b) ($\theta = 45°$)

Figure 5.3: Camping-car - the inverse Fourier transform of the S_{21} parameters at $\theta = 45°$ (a) and a comparison between the RCS results at $\theta = 45°$ (b).

In this chapter, we extended the application area of the Physical Optics (PO) approach for RCS measurements at Fresnel region distances and incidence angles higher than 20°.

We defined a field zone extrapolation factor for the diffracted field, in order to improve the accuracy of the RCS measurements.

The combination between the distance averaging technique and time gating on the inverse Fourier transforms of the scattering parameters was successfully validated as an accurate approach for RCS measurements on two flat targets, in a multipath environment.

6. Conclusions

6.1 Results

Far-field RCS measurements are affected by ground reflections or by a low signal-to-noise ratio (SNR) of the reflected wave. The radar configuration for RCS evaluation in the near-field or Fresnel zone is often very complex and near-field to far-field transformations are needed, although they are generally, time-consuming and expensive to be implemented at a large scale, and therefore not suitable for a real-time scenario. In order to overcome these shortcomings, a novel method for determining the far-field RCS from Fresnel zone measurements were developed in this work.

A mathematical model was developed with the aim to evaluate the RCS at Fresnel region ranges and a field-zone extrapolation factor between Fresnel region and far-field was calculated. Moreover, by integrating our approach with the distance averaging technique, time gating and coupling subtraction our method could be successfully applied for RCS measurements in a multipath site.

A differential approach, along with a gain and group delay calibration on the antenna system made it possible to validate our method at frequencies in the L-band, and with a pair of low-directivity antennas (Vivaldi and log-periodic antennas). The proposed approach is evaluated also with horn antennas and is based on: 1. averaging the contributions of the source points over the transmitting antenna aperture to the electric field in a specific point on the target; 2. averaging the contributions of the corresponding elementary radiator on the target to the scattered field in each field point on the receiving antenna aperture. For the particular case of antennas and target sizes comparable to the distance between target and antennas, the four-integral (for linear aperture antennas) or six-integral (for planar aperture antennas) RCS resulting expressions could be rewritten by using Fresnel integrals and the processing time was dramatically reduced, provided that Fresnel integrals can be computed asymptotically.

6.2 Original contributions

A summary of the contributions of this work is listed below:

OC1. We proposed a technique to calibrate the antenna system of a radar in terms of group delay and gain [C1, C2, C3, C8, C9], in order to perform RCS measurement in the Fresnel zone.

OC2. We proposed a new version of the distance averaging method for a radar setup [J1].

OC3. We combined our new distance averaging approach with other techniques such as coupling subtraction or time gating, in order to further reduce the effect of a multipath propagation environment [C6, C7, J2].

OC4. A new form for RCS evaluation at Fresnel zone ranges was developed, based on approximations leading to Fresnel integrals. Thus, the order of integration in the original RCS expressions was reduced and consequently, the computing time is dramatically reduced [J1].

OC5. An alternative to Fresnel to far-field transformation is proposed, based on a field zone extrapolation factor that we have developed [J2, C4].

OC6. For validation purposes, we proposed a technique for evaluating the RCS of a complex target, based on simplified small scale models. This technique allowed us to validate our approach for RCS measurements at Fresnel zone ranges on small scale models of a camping car side, a frigate, or a container house [J2].

OC7. We proposed a new PO approach for RCS evaluation at high incidence angles, including the effect of the diffraction on the target edges [C6, C7]

OC8. A field-zone extrapolation factor for high incidence angles was developed as well [J2, C6, C7].

6.3 Publications

Refereed journal papers

J1. I. V. Mihai, R. D. Tamas and A. Sharaiha, "A Technique for Radar Cross Section Measurements in the Fresnel Region," in IEEE Antennas and Wireless Propagation Letters, vol. 18, no. 6, pp. 1149-1153, June 2019 (Quartile WoS: Q1).

J2. I. V. Mihai, R. Tamas, and A. Sharaiha, "An UWB Physical Optics Approach for Fresnel-Zone RCS Measurements on a Complex Target at Non-Normal Incidence," Sensors, vol. 19, no. 24, p. 5454, Dec. 2019 (Quartile WoS: Q1).

Refereed international conferences

C1. I. V. Mihai, L. Anchidin, R. D. Tamas and A. Sharaiha, "The effect of the antenna group delay on RCS measurements in the L-band," 2018 IEEE Conference on Antenna Measurements & Applications (CAMA), Vasteras, 2018, pp. 1-2.

C2. V. Mihai, R. Tamas and A. Sharaiha, "A comparison between Vivaldi and log-periodic antenna systems for radar cross section measurements in the Fresnel region," 2019 International Workshop on Antenna Technology (iWAT), Miami, FL, USA, 2019, pp. 95-98.

C3. V. Mihai, R. Tamas and A. Sharaiha, "A Bistatic Method for Radar Cross Section Measurements in the Fresnel Region," 2019 13th European Conference on Antennas and Propagation (EuCAP), Krakow, Poland, 2019, pp. 1-5.

C4. I. V. Mihai, A. Sharaiha and R. Tamas, "UWB-Radar Cross Section Measurements in the Fresnel Region and Real Environment," 2019 International Symposium on Antennas and Propagation (ISAP), Xi'an, China, 2019, pp. 1-3.

C5. I. V. Mihai, A. Sharaiha and R. Tamas, "Radar Cross Section of a Slightly Tilted Disk in the Fresnel Region and Real Environment," 2019 IEEE Conference on Antenna Measurements & Applications (CAMA), Kuta, Bali, Indonesia, 2019, pp. 109-112.

C6. I. V. Mihai, R. Tamas and A. Sharaiha, "A Modified Physical Optics Approach for Extrapolating Fresnel Region RCS Measurements at High Incidence Angles," 2020 International Workshop on Antenna Technology (iWAT), Bucharest, Romania, 2020.

C7. I. V. Mihai, R. Tamas and A. Sharaiha, "A Technique for Including Edge Diffraction Effects on RCS Evaluation at Fresnel Region Ranges," 2020 14th European Conference on Antennas and Propagation (EuCAP), Copenhagen, Denmark, 2020.

Refereed national conferences

C8. Valentin Ilie Mihai, Liliana Anchidin, Razvan Tamas, and Ala Sharaiha "Improvement of setup calibration for radar cross section measurements ", Proc. SPIE 10977, Advanced Topics in Optoelectronics, Microelectronics, and Nanotechnologies IX, 109772S (31 December 2018);

C9. I. V. Mihai, A. Sharaiha and R. Tamas, "Mesures de la Surface Equivalente Radar dans la zone de Fresnel en environnement reeel," 21emes Journees Nationales Micro-Ondes, Caen, France, 2019, May.

Awards

P1. Winner of the **Best student paper** at *The International Workshop on Antenna Technology (iWAT)*, Miami, USA. Paper title: "A comparison between Vivaldi and log-periodic antenna systems for radar cross section measurements in the Fresnel region".

P2. Winner of the **Best student paper** at *Conference on Antenna Measurement and Applications (CAMA)*, Bali, Indonesia. Paper title: "Radar Cross Section of a Slightly Tilted Disk in the Fresnel Region and Real Environment".

P3. Winner of the **Best poster presentation** at *International Conference Advanced Topics in Optoelectronics, Microelectronics and Nanotechnologies (ATOM-N)*, Constanța, România. Paper title: "Improvement of setup calibration for radar cross section measurements".

Scientific reports throughout the doctoral studies

R1. Scientific report no. 1/2018, *Studiu privind timpul de întârziere de grup al antenelor din sistemele de măsurare a ariei efective a țintelor*;

R2. Scientific report no. 2/2019, *O nouă metodă de m ăsurare a suprafeței echivalente radar în zona Fresnel*;

R3. Scientific report no. 3/2019, *Studiu comparativ privind sistemul de antene utilizat la măsurarea suprafeței echivalente radar în zona Fresnel*;

R4. Scientific report no. 4/2019, *Măsurarea ariei echivalente unei ținte radar complexe la incidență oblică, utilizând o formă modificată a opticii ondulatorii*;

R5. Scientific report no. 5/2020, *Extrapolarea valorii ariei echivalente a unei ținte radar din zona Fresnel în zona de câmp îndepărtat, la unghiuri de incidență ridicate*;

6.4 Future research areas

Future work will focus on RCS measurements on large targets by using antennas with small apertures. Also, further study should be done on the limitations of the method in terms of the complexity of the targets with respect to the PO approximation. In a real time scenario one should also take into account the current distribution on the other parts of the target, not only on the specular side. On the other hand, it would be interesting to optimize the method and the mathematical model by taking into consideration other effects that contribute to the reflexion, such as creeping waves effect, traveling wave echo, interaction echo etc.

Bibliography

[1] J. B. Keller, "Diffraction by an aperture," *Journal of Applied Physics*, vol. 28, no. 4, pp. 426–444, 1957.

[2] R. G. Kouyoumjian and P. H. Pathak, "A uniform geometrical theory of diffraction for an edge in a perfectly conducting surface," *Proceedings of the IEEE*, vol. 62, pp. 1448–1461, Nov 1974.

[3] A. Michaeli, "Equivalent edge currents for arbitrary aspects of observation," *IEEE Transactions on Antennas and Propagation*, vol. 32, pp. 252–258, March 1984.

[4] U. P., "Approximate computation of the diffraction of plane electromagnetic waves at certain metal bodies," *Zh. Tekhn. Fiz.*, vol. 27, no. 8, pp. 1708–1718, 1957.

[5] R. Ross, "Radar cross section of rectangular flat plates as a function of aspect angle," *IEEE Transactions on Antennas and Propagation*, vol. 14, pp. 329–335, May 1966.

[6] J. W. Crispin and A. L. Maffett, "Radar cross-section estimation for simple shapes," *Proceedings of the IEEE*, vol. 53, pp. 833–848, Aug 1965.

[7] T. B. A. Senior, "A survey of analytical techniques for cross-section estimation," *Proceedings of the IEEE*, vol. 53, pp. 822–833, Aug 1965.

[8] M. E. Bechtel, "Application of geometric diffraction theory to scattering from cones and disks," *Proceedings of the IEEE*, vol. 53, pp. 877–882, Aug 1965.

[9] G. Thiele and T. Newhouse, "A hybrid technique for combining moment methods with the geometrical theory of diffraction," *IEEE Transactions on Antennas and Propagation*, vol. 23, pp. 62–69, January 1975.

[10] Shung-Wu Lee, "Comparison of uniform asymptotic theory and ufimtsev's theory of electromagnetic edge diffraction," *IEEE Transactions on Antennas and Propagation*, vol. 25, pp. 162–170, March 1977.

[11] T. Griesser and C. Balanis, "Backscatter analysis of dihedral corner reflectors using physical optics and the physical theory of diffraction," *IEEE Transactions on Antennas and Propagation*, vol. 35, pp. 1137–1147, October 1987.

[12] S. K. Wong, E. Riseborough, G. Duff, and K. K. Chan, "Radar cross-section measurements of a full-scale aircraft duct/engine structure," *IEEE Transactions on Antennas and Propagation*, vol. 54, pp. 2436–2441, Aug 2006.

[13] A. Schroder, M. Renker, U. Aulenbacher, A. Murk, U. Boniger, R. Oechslin, and P. Wellig, "Numerical and experimental radar cross section analysis of the quadrocopter dji phantom 2," in *2015 IEEE Radar Conference*, pp. 463–468, Oct 2015.

[14] T. Dogaru and C. Kenyon, "Numeric computation of the radar cross section of in-flight projectiles," tech. rep., US Army Research Laboratory, 11 2016.

[15] Y.-K. K. Yi-Ru Jeong, Chan-Sun Park and J.-G. Yook, "Analysis of rcs of low observable aircraft in vhf band," *International Journal of Antennas and Propagation,*, pp. 1–10, 2018.

[16] D. W. Richardson, R. P. Ortega, and S. N. Tabet, "Monostatic rcs for general aviation aircraft," in *2018 International Applied Computational Electromagnetics Society Symposium (ACES)*, pp. 1–2, March 2018.

[17] E. F. Knott, "A progression of high-frequency rcs prediction techniques," *Proceedings of the IEEE*, vol. 73, pp. 252–264, Feb 1985.

[18] T. T. Moon and P. W. Taliana, "Rcs measurements in multipath environments," in *AMPC Asia-Pacific Microwave Conference,*, vol. 2, pp. 799–801, Aug 1992.

[19] S. Li, B. Zhu, and H. Sun, "Nufft-based near-field imaging technique for far-field radar cross section calculation," *IEEE Antennas and Wireless Propagation Letters*, vol. 9, pp. 550–553, 2010.

[20] S. Scherr, R. Afroz, S. Ayhan, S. Thomas, T. Jaeschke, S. Marahrens, A. Bhutani, M. Pauli, N. Pohl, and T. Zwick, "Influence of radar targets on the accuracy of fmcw radar distance measurements," *IEEE Transactions on Microwave Theory and Techniques*, vol. 65, pp. 3640–3647, Oct 2017.

[21] R. D. Tamas, D. Deacu, G. Vasile, and C. Ioana, "A method for antenna gain measurements in nonanechoic sites," *Microwave and Optical Technology Letters*, vol. 56, no. 7, pp. 1553–1557, 2014.

[22] L. Corucci, E. Giusti, M. Martorella, and F. Berizzi, "Near field physical optics modelling for concealed weapon detection," *IEEE Transactions on Antennas and Propagation*, vol. 60, pp. 6052–6057, Dec 2012.

[23] C. Bourlier and P. Pouliguen, "Useful analytical formulae for near-field monostatic radar cross section under the physical optics: Far-field criterion," *IEEE Transactions on Antennas and Propagation*, vol. 57, pp. 205–214, Jan 2009.

[24] R. F. Millar, "An approximate theory of the diffraction of an electromagnetic wave by an aperture in a plane screen," *Proceedings of the IEE - Part C: Monographs*, vol. 103, pp. 177–185, March 1956.